Computers and Mathematics with Applications 56 (2008) 2596–2608

Contents lists available at ScienceDirect

Computers and Mathematics with Applications

journal homepage: www.elsevier.com/locate/camwa

Visualization of heat transport using dimensionless heatfunction for natural convection and conduction in an enclosure with thick solid ceiling

Moghtada Mobedi [a], Hakan F. Oztop [b,*]

[a] Department of Mechanical Engineering, Izmir Institute of Technology, Urla, TR-35430, Izmir, Turkey

[b] Department of Mechanical Engineering, Fırat University, TR-23119, Elazig, Turkey

ARTICLE INFO

Article history:
Received 24 January 2008
Received in revised form 10 May 2008
Accepted 27 May 2008

Keywords:
Dimensionless heatfunction
Conjugate heat transfer
Natural convection
Heat transport
Heatline

ABSTRACT

A conjugate conduction-(natural)convection problem is numerically studied in order to present the application of dimensionless heatfunction for entire computational domain including solid and fluid regions in an enclosure with thick solid ceiling. The modified dimensionless heatfunction for solid region is defined to provide continuity of dimensionless heatfunction on solid–fluid interface. The enclosure is differentially heated from vertical walls, and horizontal walls are adiabatic. Finite difference method is employed to solve the set of governing equations. The dimensionless governing parameters for computations are: Rayleigh number (from 10^3 to 10^6), dimensionless ceiling wall thickness (0.05 and 0.5) and thermal conductivity ratio (from 1 to 100). The obtained results shows that the heat and fluid flows in the enclosure are considerably influenced by Rayleigh number and thermal conductivity ratio. Dimensionless wall thickness comparatively has less effect on heat transfer rate through the cavity.

1. Introduction

Natural convection in enclosures is an area of interest due to its great importance in engineering applications as reviewed by Ostrach [1,2]. The studies on natural convection in enclosures in the literature can be divided mainly to two groups. In the first group, natural convection due to a uniformly/non-uniformly heated wall with zero thickness [3] and in the second group, natural convection in the enclosures with finite thickness wall/walls are studied. In the solution of second group, convection and conduction (and/or radiation) heat transfer modes occur in enclosure [4–14].

The problem of natural convection heat transfer in an enclosure with finite thickness wall/walls was investigated in different configurations for four sides thick walls by Kim and Viskanta [4], for turbulent flow by Ben Yedder and Bilgen [5], inclined laminar flow by Ben Yedder and Bilgen [6], for a vertical thick wall by Kaminski and Prakash [7], for porous media filled enclosure with a thick wall and for a sandwich panel by Saeid [8,9]. Sanchez et al. [10] made experimental and numerical analysis to obtain the effect of thick walls on heat transfer in an enclosure with heated from bottom wall. Turkoglu and Yucel [11] investigated the effect of partition number on heat transfer and flow fields for a conjugate natural convection.

The problem of thermal bridging is widely faced in industrial applications, particularly in building envelopes, metal casing panels, metal profiles, and window frames. A thermal bridge increases heat transfer between two walls and creates local temperature gradients on walls, which may cause condensation problems on the wall surfaces. The transfer of heat through a thermal bridge has been investigated by Larbi [12] and Ben Nakhi [13]. A temperature factor or thermal leakage coefficient was developed to measure the effect of a thermal bridge by Song et al. [14]. Table 1 shows samples of the different solid

* Corresponding author. Tel.: +90 424 237 0000x5328; fax: +90 424 241 5526.
E-mail address: hfoztop1@gmail.com (H.F. Oztop).

0898-1221/$ – see front matter © 2008 Elsevier Ltd. All rights reserved.
doi:10.1016/j.camwa.2008.05.009

Nomenclature

d	wall thickness, m
D	dimensionless wall thickness, d/L
g	acceleration of gravity, m/s^2
h	dimensional heatfunction, W/m
H	dimensionless heatfunction for fluid, $H_f = h/(k_f\,(T_h - T_c))$
H^*	modified dimensionless heatfunction for solid, $H_s = h/(k_s(T_h - T_c))$
k	thermal conductivity, W/mK
K	thermal conductivity ratio, k_s/k_f
L	length or height of enclosure, m
Nu	local Nusselt number
$\bar{N}u$	average Nusselt number
Pr	Prandtl number
Ra	Rayleigh number based on enclosure length
t	physical time, s
T	temperature, K
u, v	velocity components in x and y directions, m/s
U, V	dimensionless velocity components in X and Y directions
x, y	dimensional Cartesian coordinate, m
X, Y	dimensionless Cartesian coordinate

Greek symbols

α	thermal diffusivity, m^2/s
α^*	dimensionless thermal diffusivity ratio, α_S/α_f
β	thermal expansion coefficient, K^{-1}
δ	interval
Ω	dimensionless vorticity
θ	dimensionless temperature
τ	dimensionless time
Ψ	dimensionless stream function

Subscripts

c	cold
f	fluid
h	hot
s	solid
L	enclosure length

Table 1
Different fluid-solid pairs and their thermal conductivity ratio [15]

Fluid	K_f (W/m K)	Solid	K_S (W/m K)	K_S/K_f
Liquid water	0.613	Polystyrene	0.027	0.044
Vapor water	0.019	Glass	1.400	73.68
Air	0.026	Plywood	0.120	4.615
Engine oil	0.1450	Steel, AISI 304	15.10	104.1

material which may be used for cavity walls and fluid materials which may exist inside a cavity. As we can, the value of thermal conductivity ratio can be widely changed.

In all of above studies, isotherms are used to show temperature distribution in a domain. However, it is not easy to realize the direction of heat transfer since heat flux is not perpendicular to isotherm in a convective flow. Heatline is a useful tool for visualization and analysis of not only direction but also intensity of heat flux in a domain. They provide corridors where heat is transferred from a hot to a cold region by convection and/or conduction.

Heatfunction was originally introduced by Kimura and Bejan [16] for a natural convection in a differentially heated square enclosure whose top and bottom boundaries were insulated. Then, the massline concept was proposed to the convective mass transfer problems [17]. There are studies in which heatlines were applied to pure convective heat flows [18–20] or convection heat transfer in a porous medium [21]. A detailed study was performed by Costa [22] to present the application of heatlines on various heat and mass transfer problems. He showed that heatlines can be applied to the boundary layer

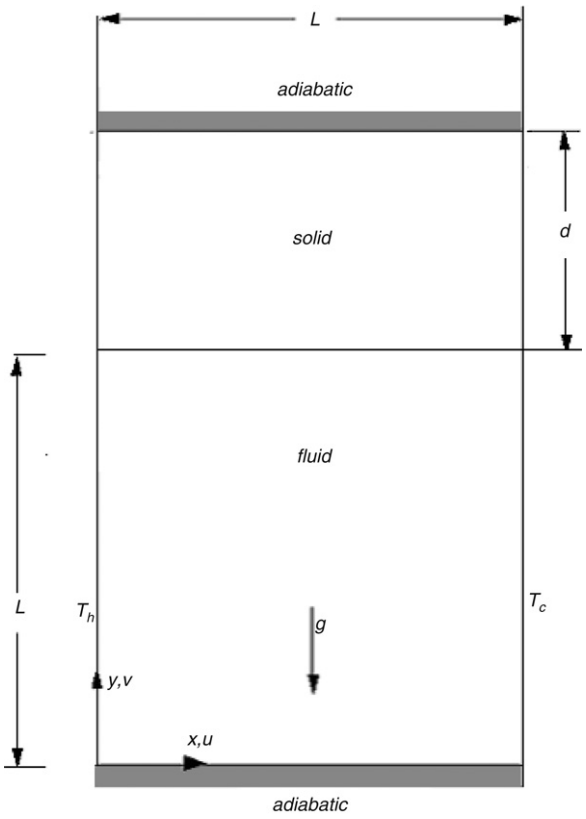

Fig. 1. The schematic view of the considered problem.

problems, turbulent flow, reacting flow, fluid-saturated porous media for both isotropic and anisotropic media. Costa [23] also unified streamline, heatline and mass transfer methods in order to become as a common treatment. Recently, Dalal and Das [24] visualized the heat transport used heatline technique for complicated enclosure. They observed that heat transport is slightly affected by undulation of the wall.

The main aim of this study is to suggest a method for determination of dimensionless heatfunction in conjugate conduction-convection heat transfer problems. Although, the unification of heatfunction for anisotropic media was derived by Costa [23], in the present study, two dimensionless heatfunction equations, one for fluid inside the enclosure and the other, which is proposed as modified dimensionless heatfunction, for solid ceiling are suggested. Both dimensionless heatfunctions have the same definition at solid–fluid interface, hence the continuity of dimensionless heatfunction on the solid–fluid interface is provided. The heatfunction equations are non-dimensionalized by employing the same dimensionless parameters which are used for non-dimensionalizing of the main governing equations. Both the intensity and direction of dimensionless heat flux on the interface can be visualized by the proposed method. The derivation of boundary conditions for dimensionless heatfunction equations is also presented. The benefits of dimensionless heatline visualization in conjugate conduction-convection heat transfer are revealed. Furthermore, the effects of dimensionless governing parameters which are Rayleigh number, thermal conductivity ratio and dimensionless wall thickness on the heat and fluid flow inside the cavity are presented.

2. The considered problem

The problem is schematically shown in Fig. 1 which is a square enclosure with a side length of L. The upper horizontal wall (ceiling) has finite thickness which is defined with d. The dimensionless thickness of ceiling wall is 0.05 and 0.5 in the present study. Both top surface of the ceiling and bottom surface of the enclosure are insulated. The vertical walls of the enclosure are maintained at different T_h (hot) and T_c (cold) constant temperatures such that $T_h > T_c$. The heat transfer in the enclosure occurs by laminar natural convection.

3. Mathematical formulation

The governing equations for the problem are continuity, momentum and energy equations for fluid inside the enclosure. The unsteady forms of the governing equations are solved to obtain steady state results. The pressure term in the

momentum equation can be eliminated if vorticity-stream function approach is used. Gravity acts in vertical direction and the radiation effects are neglected with respect to other modes of heat transfer. By employing the dimensionless vorticity and streamfunction parameters, the dimensionless forms of governing equations can be written as:

$$\frac{\partial \Omega}{\partial \tau} + \frac{\partial U\Omega}{\partial X} + \frac{\partial V\Omega}{\partial Y} = Pr\left(\frac{\partial^2 \Omega}{\partial X^2} + \frac{\partial^2 \Omega}{\partial Y^2}\right) + Ra.Pr.\frac{\partial \theta_f}{\partial X} \tag{1}$$

$$\frac{\partial^2 \Psi}{\partial X^2} + \frac{\partial^2 \Psi}{\partial Y^2} = -\Omega \tag{2}$$

$$\frac{\partial \theta_f}{\partial \tau} + \frac{\partial U\theta_f}{\partial X} + \frac{\partial V\theta_f}{\partial Y} = \frac{\partial^2 \theta_f}{\partial X^2} + \frac{\partial^2 \theta_f}{\partial Y^2} \tag{3}$$

where U, V, θ, τ, X and Y are dimensionless parameters as:

$$X = \frac{x}{L}, \qquad Y = \frac{y}{L}, \qquad U = \frac{uL}{\alpha_f}, \qquad V = \frac{vL}{\alpha_f}, \qquad \theta_f = \frac{(T_f - T_c)}{(T_h - T_c)}, \qquad \tau = \frac{\alpha_f t}{L^2}. \tag{4}$$

The dimensionless vorticity, stream function, Rayleigh number and Prandtl number are defined as:

$$\Omega = \frac{\partial V}{\partial X} - \frac{\partial U}{\partial Y} \tag{5}$$

$$U = \frac{\partial \Psi}{\partial Y}, \qquad V = -\frac{\partial \Psi}{\partial X} \tag{6}$$

$$Ra = \frac{g\beta(T_h - T_C)L^3}{\nu\alpha_f}, \qquad Pr = \frac{\nu}{\alpha_f}. \tag{7}$$

Based on the defined dimensionless parameters, the dimensionless form of heat conduction equation for the horizontal wall becomes as:

$$\frac{\partial \theta_S}{\partial \tau} = \alpha_S^*\left(\frac{\partial^2 \theta_S}{\partial X^2} + \frac{\partial^2 \theta_S}{\partial Y^2}\right) \tag{8}$$

where $\theta_s = (T_s - T_c)/(T_h - T_c)$ and α_S^* are ceiling wall dimensionless temperature and thermal diffusivity ratio (α_S/α_f). The boundary conditions for the domain which is shown in Fig. 1 can be written as follows:

$$Y = 0 \qquad \Omega = -\frac{\partial U}{\partial Y}, \qquad \Psi = \frac{\partial \theta_f}{\partial Y} = 0 \tag{9}$$

$$Y = 1 + D \qquad \Omega = \Psi = \frac{\partial \theta_S}{\partial Y} = 0 \tag{10}$$

$$X = 0, X = 1 \qquad \Omega = \frac{\partial V}{\partial X}, \qquad \Psi = 0, \qquad \theta_f(0, Y, \tau) = 1, \qquad \theta_f(1, Y, \tau) = 0 \tag{11}$$

$$Y = 1 \qquad \Omega = -\frac{\partial U}{\partial Y}, \qquad \Psi = 0, \qquad \theta_S = \theta_f \quad \text{and} \quad K\left.\frac{\partial \theta_S}{\partial Y}\right|_S = \left.\frac{\partial \theta_f}{\partial Y}\right|_f. \tag{12}$$

The thermal conductivity ratio and dimensionless wall thickness are shown by K and D, respectively. The following initial values for the dimensionless temperature, vorticity and stream function are used:

$$U = V = \Omega = \Psi = \theta_f = \theta_S = 0. \tag{13}$$

The dimensionless forms of the governing equations and boundary conditions reduce the number of governing parameters to five which are Ra, Pr, K, α^* and D. Since the steady results are concerned in the present study, the thermal diffusivity ratio does not play a role on the obtained results. The present study is performed for air with $Pr = 0.71$. Thus, the effects of three dimensionless parameters which are Rayleigh number, thermal conductivity ratio and dimensionless wall thickness are investigated.

4. Definition of dimensionless heatfunction equation

The problem considered has solid and fluid regions which are physically separated by interface. The heatfunction equations were applied to the steady temperature and velocity distributions. Although the dimensional heatfunction for both solid and fluid regions are the same, the dimensionless heatfunction is different. The definitions of dimensionless heatfunctions for solid and fluid regions are separately discussed in this section.

4.1. Dimensionless heatfunction equation for fluid

Heatfunction for a dimensional convection problem is defined as

$$-\frac{\partial h}{\partial x} = \rho c_P v(T_f - T_C) - k_f \frac{\partial T_f}{\partial y} \tag{14}$$

$$\frac{\partial h}{\partial y} = \rho c_P u(T_f - T_C) - k_f \frac{\partial T_f}{\partial x} \tag{15}$$

where h is the dimensional heatfunction. By employing the dimensionless parameters defined in Eq. (4), the Eqs. (14) and (15) can be written in dimensionless form:

$$-\frac{\partial H_f}{\partial X} = V\theta_f - \frac{\partial \theta_f}{\partial Y} \tag{16}$$

$$\frac{\partial H_f}{\partial Y} = U\theta_f - \frac{\partial \theta_f}{\partial X} \tag{17}$$

H_f is dimensionless heatfunction for the fluid and it is defined based on the fluid thermal conductivity:

$$H_f = \frac{h}{(T_h - T_c)k_f}. \tag{18}$$

By assuming H_f is a continuous function to its second order derivative, the following dimensionless heat function can be obtained:

$$\frac{\partial^2 H_f}{\partial X^2} + \frac{\partial^2 H_f}{\partial Y^2} = \frac{\partial U\theta_f}{\partial Y} - \frac{\partial V\theta_f}{\partial X}. \tag{19}$$

This is a Poisson equation which can be solved numerically. The convection terms which are written on the right side act as a source term. The solution of this equation yields dimensionless heatfunction of fluid region. The drawing of isolines of heatfunction provides heatlines.

4.2. Dimensionless heatfunction equation for solid region

The dimensional definition of heatfunction for the solid region is:

$$-\frac{\partial h}{\partial x} = -k_S \frac{\partial T_S}{\partial y} \tag{20}$$

$$\frac{\partial h}{\partial y} = -k_S \frac{\partial T_S}{\partial x}. \tag{21}$$

By employing the dimensionless parameters of Eq. (4), the dimensionless form of Eqs. (20) and (21) can be found as:

$$-\frac{\partial H_S}{\partial X} = -\frac{\partial \theta_S}{\partial Y} \tag{22}$$

$$\frac{\partial H_S}{\partial Y} = -\frac{\partial \theta_S}{\partial X} \tag{23}$$

where θ_S dimensionless temperature in the ceiling wall. H_S represents dimensionless heatfunction for solid region which is defined based on solid thermal conductivity:

$$H_S = \frac{h}{(T_h - T_c)k_S}. \tag{24}$$

The comparison between the definitions of solid and fluid dimensionless heatfunctions, (Eqs. (19) and (24)) shows that the values of H_S and H_f are not the same on the solid–fluid interface and a discontinuity exits. A point on the interface has two dimensionless heatfunction values due to different definitions of H_S and H_f. A modified heatfunction for solid region may be a solution for this difficulty and it can be defined as:

$$H_S^* = H_S K = \frac{h}{(T_h - T_c)k_f}. \tag{25}$$

Comparison of the modified heatfunction equation for solid region (Eq. (25)) and the dimensionless heatfunction for fluid region (Eq. (19)) shows that $H_S^* = H_f$ at the solid–fluid interface. The definition of the modified dimensionless heatfunction can be explained as a dimensionless heatfunction of solid region based on fluid thermal conductivity. It provides a continuous heatfunction between solid and fluid on the interface. The Eqs. (22) and (23) can be revised by using the definition of the modified heatfunction for solid region:

$$-\frac{\partial H_S^*}{\partial X} = -K\frac{\partial \theta_S}{\partial Y} \tag{26}$$

$$\frac{\partial H_S^*}{\partial Y} = -K\frac{\partial \theta_S}{\partial X}. \tag{27}$$

Taking derivatives of Eqs. (26) and (27) with respect to X and Y yields the following modified heatfunction equation for solid region:

$$\frac{\partial^2 H_S^*}{\partial X^2} + \frac{\partial^2 H_S^*}{\partial Y^2} = 0. \tag{28}$$

The solution of the above equation yields distribution of the modified dimensionless heatfunction in the solid region. The Eqs. (28) and (19) can be unified; however we prefer to use a different notation, by which readers can tell the difference between H_S^* and H_S.

4.3. Boundary conditions for dimensionless heatfunction equations

The boundary conditions for Eqs. (19) and (28) are obtained from the integration of differential definition of H_S^* and H_f along the considered boundary. For example, for $X = 0$ boundary;

$$\text{for } 0 < Y \leq 1 \quad H_f(0, Y) = H_f(0, 0) - \int_0^Y \frac{\partial \theta_f}{\partial X} \mathrm{d}Y \tag{29}$$

$$\text{for } 1 < Y \leq 1 + D \quad H_S^*(0, Y) = H_S^*(0, 1) - \int_1^Y K\frac{\partial \theta_S}{\partial X} \mathrm{d}Y \tag{30}$$

where in this study at $Y = 0, H_f(X, 0) = 0$ is considered. For the upper solid–fluid interface, the direction of heat exchanged between the solid and fluid is perpendicular to the interface. Hence, the boundary condition for dimensionless heatfunction equations at the interface can be determined as:

$$\text{for } Y = 1 \text{ and } 0 \leq X \leq 1 \quad H_f(X, 1) = H_f(0, 1) + \int_0^X \frac{\partial \theta_f}{\partial Y} \mathrm{d}X. \tag{31}$$

5. Numerical solution procedure

The set of governing equations is solved by starting from an initial state. The vorticity equation is solved for a time step to compute the vorticity field in the computational domain. Then, the stream function equation is solved and the velocity values are obtained from the stream function field. At the same time step and by using the new values of velocity, the energy equation is solved and the temperature field is computed. The procedure is continued until the steady state is reached [25, 26]. The energy and vorticity equations are solved line by line by employing ADI method, whereas the stream function is solved point by point. The finite difference forms of diffusion and convection terms are written based on the three points central difference which has a second order accuracy.

The governing equations for fluid flow (Eqs. (1)–(3)) are solved for the entire computational domain. As indicated earlier, the value of the Prandtl number for flow region is assigned as $Pr = 0.71$ while for the solid region it is changed to $Pr = 10^{20}$. This change of Prandtl number value causes the vorticity, stream function and velocity values in the ceiling wall become zero and consequently the convection heat transfer equation is simplified to the heat conduction equation for the solid wall. The backward and forward differences for temperature gradients on the solid–fluid interface are used to determine the interface temperature. The vorticity values on the solid boundaries are calculated by using the relation developed by Wong and Baker [27]. The convergence criterion for the solution procedure is defined as:

$$\frac{\sum \left|\theta^{n+1} - \theta^n\right|}{\Delta\tau \sum \theta^n} \leq 10^{-4}. \tag{32}$$

The total relative error is divided by dimensionless interval time; hence the convergence criterion is the relative total error per unit of dimensionless time. The numerical checks showed that the convergence criterion used is appropriate to obtain accurate results.

The local and average Nusselt number values for $X = 0$ and $X = 1$ boundaries of enclosure are calculated by the following equations:

$$Nu|_{X=0 \text{ or } 1} = -\left.\frac{\partial \theta_f}{\partial X}\right|_{X=0 \text{ or } 1} \tag{33}$$

$$\bar{N}u|_{X=0 \text{ or } 1} = \int_{Y=0}^{Y=1} \left. Nu \right|_{X=0 \text{ or } 1} \mathrm{d}Y. \tag{34}$$

Table 2
Comparison of the present numerical results with the Benchmark [3]

Ra	de Vahl Davis and Jones [3]		Present study	
	$\lvert\psi\rvert_{max}$	$\bar{N}u$	$\lvert\psi\rvert_{max}$	$\bar{N}u$
10^3	–	1.118	1.174	1.114
10^4	–	2.243	5.109	2.240
10^5	9.612	4.519	9.693	4.510
10^6	16.750	8.800	16.916	8.803

Table 3
Comparison between the obtained results with Kaminski et al. solution [7]

Ra	K	Kaminski et al. $\bar{N}u$	Present study $\bar{N}u$
7.1×10^2	1	0.87	0.866
	∞	1.06	1.062
7.1×10^4	1	2.08	2.074
	∞	4.08	4.034
7.1×10^5	1	2.87	2.850
	∞	7.99	7.911

By the same way, the local and average Nusselt number for the solid–fluid ceiling interface is defined as:

$$Nu|_{Y=1} = -\left.\frac{\partial\theta_f}{\partial Y}\right|_{Y=1} \tag{35}$$

$$\bar{N}u|_{Y=1} = \int_{X=0}^{X=1} Nu\Big|_{Y=1} \mathrm{d}X. \tag{36}$$

Non-uniform mesh was used both for the fluid and solid regions. The grid sizes were selected fine near walls. They were expanded continuously towards the center of enclosure. The number of nodes in X and Y directions was 80×140 in which 80×60 nodes were used in the upper horizontal wall. The smallest grid spacing which was in fluid region near to the solid walls was 0.0005.

5.1. Validation of code and computation

In order to validate the employed method and check the written program, results for pure natural convection in an air filled square enclosure were obtained and compared with the benchmark solution of de Vahl Davis and Jones [3]. Table 2 shows the comparison between two solutions. For the check of conjugate solution accuracy, the solution for the problem which was studied by Kaminski and Prakash [7] were obtained. The comparison is shown in Table 3. The average Nusselt Number given in these tables was defined in the related references. A good agreement between the obtained and reported results can be observed.

6. Results and discussion

Flow and temperature fields, heat transfer rate and heat transport visualization are examined for different values of Rayleigh number, thermal conductivity ratio and wall thickness ratio in a differentially heated enclosure with thick ceiling. Results are presented with streamlines, isotherms and heatlines for these parameters.

Fig. 2(a–c) show streamlines (on the left), isotherms (on the middle) and heatlines (on the right) in an enclosure with a thick horizontal top wall, $D = 0.5$, and low thermal conductivity ratio, $K = 1$, for three different values of Rayleigh number, $Ra = 10^3$, 5×10^4 and 10^6. Intervals for streamfunction, temperature and heatfunction are also given. For $Ra = 10^3$, the heatlines are uniformly distributed inside the enclosure which indicates a weak convection heat transport. Single circulation cells are formed in clockwise rotating direction as shown by streamlines. Heat conduction in the horizontal wall is almost one dimensional since the effect of convection on the solid–fluid interface is weak. The isotherms are distributed almost parallel to the vertical wall inside the solid due to domination of conduction heat transfer. Similarly, the heatlines are parallel to the horizontal walls in the fluid region. The streamlines elongate inside the enclosure for higher Rayleigh number, namely $Ra = 5 \times 10^4$ due to increase of convection. For $Ra = 10^6$, non-uniform streamlines and heatlines form and this non-uniformity implies strong convection in the outer region of the cavity center. Isotherms are almost parallel to the horizontal wall in the center of the fluid region. A two dimensional heat transfer occurs in the horizontal wall since convective heat transfer on the interface of enclosure becomes strong. Thus, heatlines are cumulated near the vertical and top wall of the fluid-filled enclosure.

The streamlines, isotherms and heatlines of enclosure with $K = 100$ and $D = 0.5$ for different Rayleigh numbers as $Ra = 10^3$, 5×10^4 and 10^6 are presented in Fig. 3. The strong one-dimensional conduction heat transfer in the horizontal wall can be easily observed from heatline contours since heatlines in the solid wall are denser than those in the fluid region.

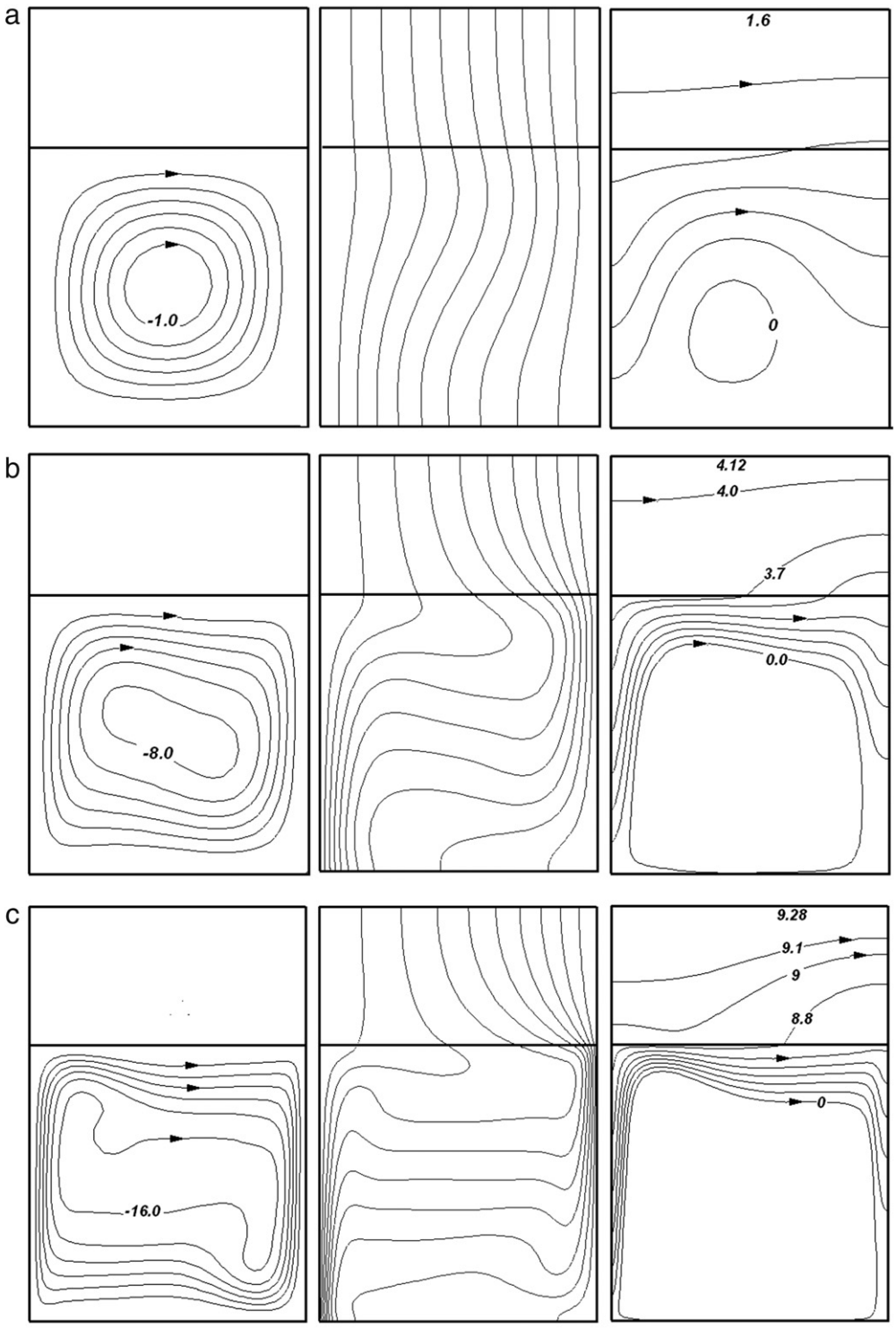

Fig. 2. Streamlines (on the left), isotherms (on the middle) and heatlines (on the right) in a cavity with $D = 0.5$ and $K = 1$, (a) $Ra = 10^3$, ($\delta\psi = -0.17$, $\delta\theta = 0.1, \delta H = 0.27$), (b) $Ra = 5 \times 10^4$, ($\delta\psi = -0.17, \delta\theta = 0.1, \delta H = 0.69$), ($H = 3.7, 4.0$ were added) (c) $Ra = 10^6$ ($\delta\psi = -0.17, \delta\theta = 0.1, \delta H = 1.55$) ($H = 8.8, 9.0, 9.1$ were added).

The modified dimensionless heatfunction for solid region provides a powerful means to compare the dimensionless heat transfer in solid and fluid regions. The increase of the Rayleigh number enhances the convective heat transfer, however it can not become as a dominant heat transfer mode on the solid–fluid interface. Hence, conduction heat transfer is one

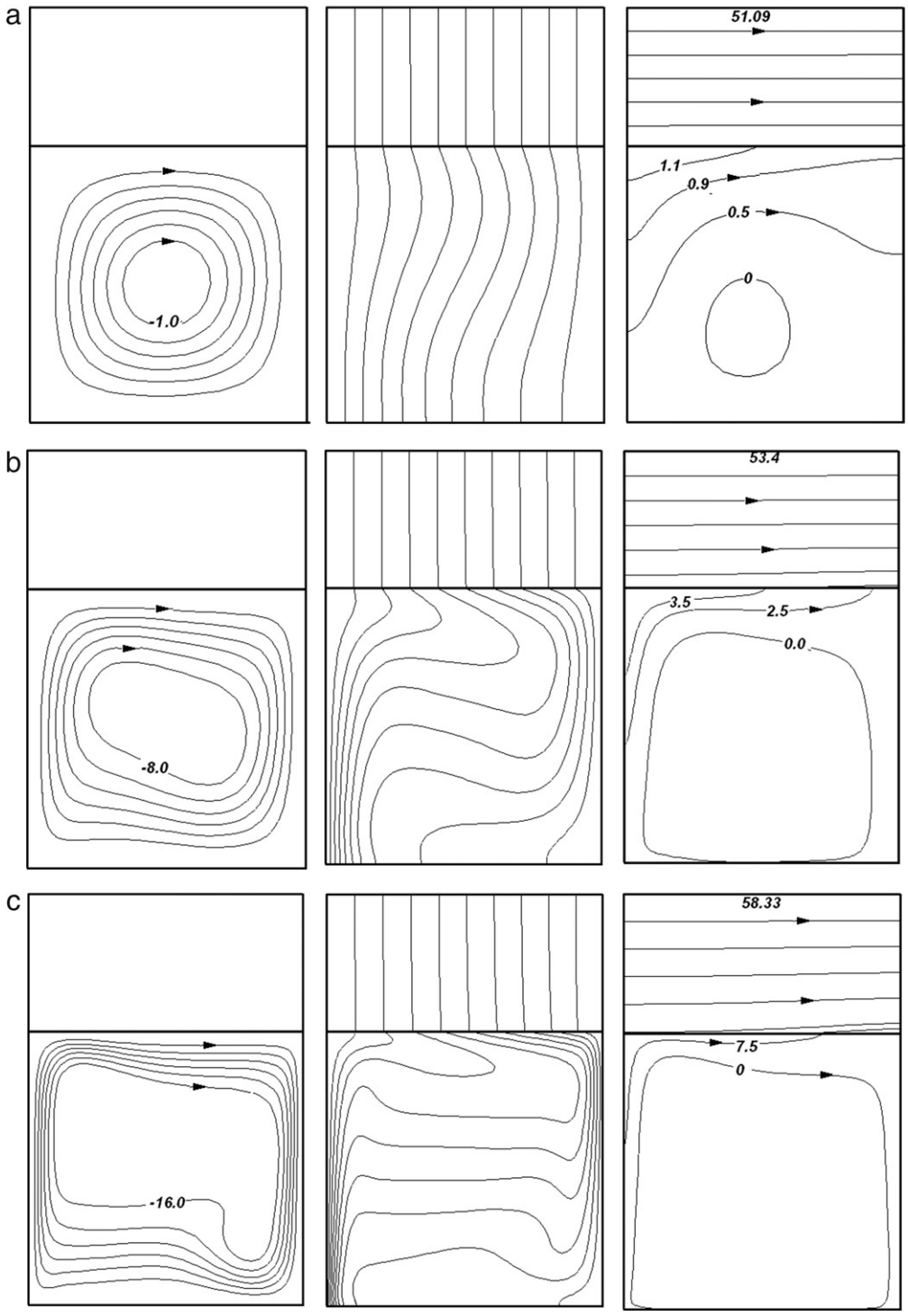

Fig. 3. Streamlines (on the left), isotherms (on the middle) and heatlines (on the right) in a enclosure with $D = 0.5$ and $K = 100$, (a) $Ra = 10^3$, ($\delta\psi = -0.17, \delta\theta = 0.1, \delta H = 8.52$) ($H = 0.5, 0.9, 1.1$ were added) (b) $Ra = 5 \times 10^4$, ($\delta\psi = -0.17, \delta\theta = 0.1, \delta H = 8.9$) ($H = 2.5, 3.5$ were added) (c) $Ra = 10^6$, ($\delta\psi = -0.17, \delta\theta = 0.1, \delta H = 9.72$) ($H = 7.5$ was added).

dimensional in the horizontal wall even for $Ra = 10^6$. Table 4 indicates the values of average Nu number of the hot and cold walls and maximum absolute streamfunction for two conductivity ratios ($K = 1$ and $K = 100$) and two different wall thicknesses ($D = 0.05$ and $D = 0.5$). The comparison of $\bar{N}u|_{X=0}$ (hot wall), $\bar{N}u|_{X=1}$ (cold wall) and $|\psi|_{\max}$ of the cavities with $K = 1$ and $K = 100$ reveals that the increase of conductivity ratio has two effects. Firstly, it enhances the convection heat

Table 4
The values of average Nusselt number of hot and cold vertical walls and maximum absolute values of stream function for $Ra = 10^6$, $K = 1$, 100 and $D = 0.05, 0.5$

$K = 1$		$K = 100$	
$D = 0.05$	$D = 0.5$	$D = 0.05$	$D = 0.5$
$\lvert\psi\rvert_{max} = 17.20$	$\lvert\psi\rvert_{max} = 17.46$	$\lvert\psi\rvert_{max} = 19.13$	$\lvert\psi\rvert_{max} = 19.73$
$\bar{N}u\lvert_{X=0} = 8.89$	$\bar{N}u\lvert_{X=0} = 8.98$	$\bar{N}u\lvert_{X=0} = 9.41$	$\bar{N}u\lvert_{X=0} = 9.53$
$\bar{N}u\lvert_{X=1} = 8.43$	$\bar{N}u\lvert_{X=1} = 7.98$	$\bar{N}u\lvert_{X=1} = 6.36$	$\bar{N}u\lvert_{X=1} = 6.06$

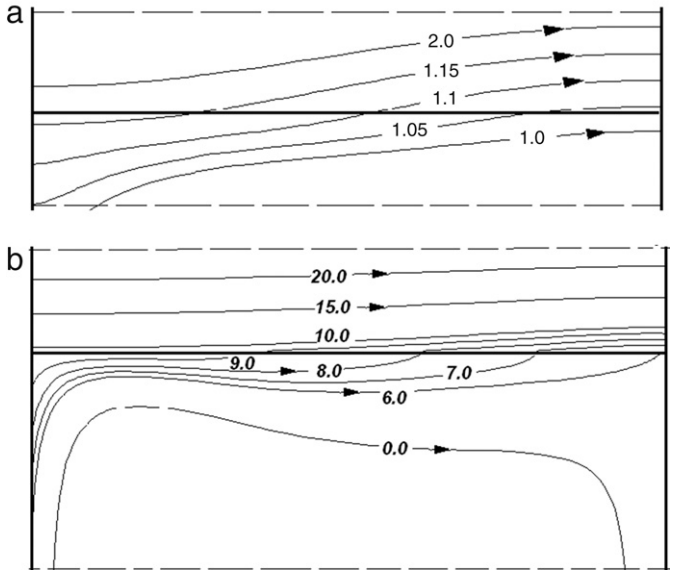

Fig. 4. Heatlines on the solid–fluid interface regions in enclosures with $D = 0.5$ (a) $Ra = 10^3$, $K = 1$ (b) $Ra = 10^6$, $K = 100$.

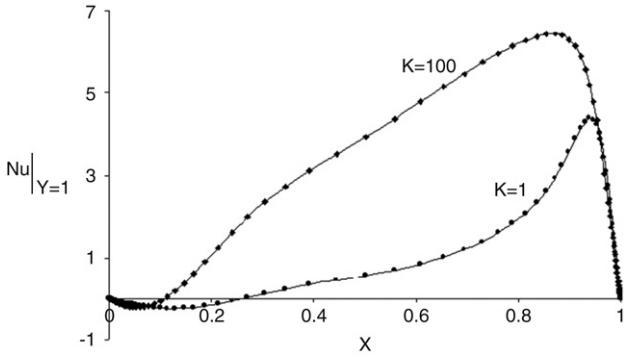

Fig. 5. Variation of local Nusselt number along the solid–fluid interface for enclosure with $Ra = 10^6$ and $D = 0.5$.

transport in the enclosure since the values of $|\psi|$ and $\bar{N}u|_{X=0}$ (hot wall) are increased. Secondly, it increases heat transfer between the ceiling wall and fluid since the value of $\bar{N}u|_{X=1}$ (cold wall) is decreased.

As seen in Figs. 2 and 3, the dimensionless heatlines are perpendicular to the isotherms in solid region since no convective heat flow exists. The dimensionless heatfunction is continuous on the interface. An enlarged view of heatlines on the solid–fluid interface regions can be seen in Fig. 4 for enclosure with $D = 0.5$. Fig. 4(a) shows heatlines for $K = 1$ and $Ra = 10^3$, and Fig. 4(b) depicts heatlines for $K = 100$ and $Ra = 10^6$. The heatline patterns provide detailed views for visualization of direction and intensity of dimensionless heat flux at the interface. The difference in values of heatlines denotes dimensionless heat flux between the heatlines. For most of interface region, heat is transferred from fluid to solid. The comparison between the heatlines of two interfaces shows that for $K = 100$, the rate of dimensionless heat transfer from fluid to solid is considerably greater than $K = 1$.

The increase of the heat transfer between the ceiling wall and fluid with increase of thermal conductivity ratio can be observed in Fig. 5 where the variations of local Nusselt number along the interface for $K = 1$ and $K = 100$ are illustrated.

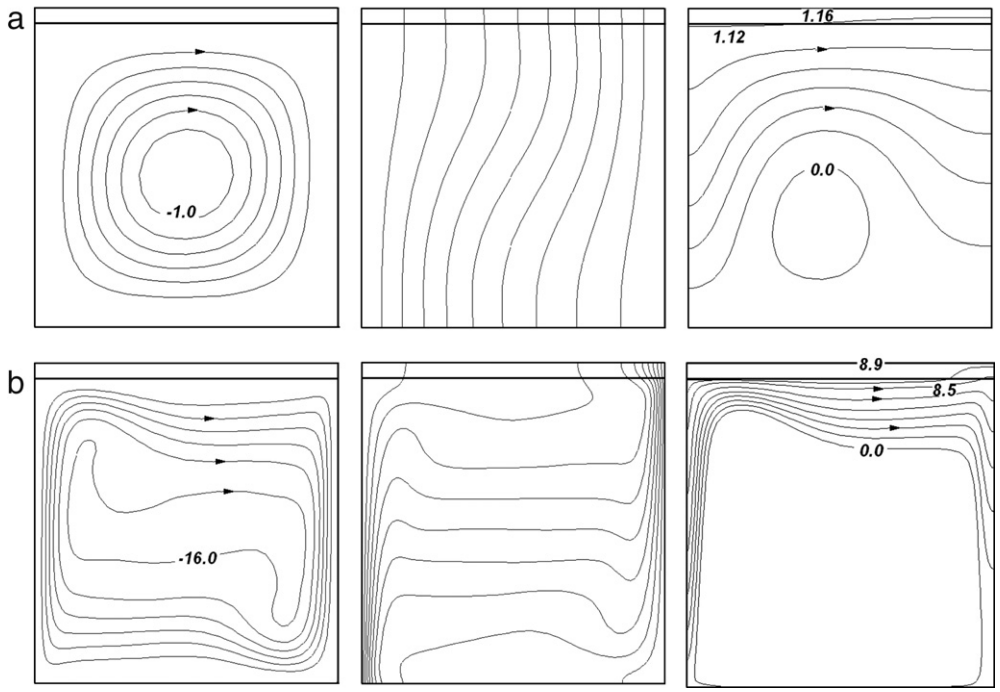

Fig. 6. Streamlines (on the left), isotherms (on the middle) and heatlines (on the right) in the enclosure with $D = 0.05$ and $K = 1$ (a) $Ra = 10^3$, ($\delta\psi = -0.17, \delta\theta = 0.1, \delta H = 0.19$) ($H = 1.12$ was added) (b) $Ra = 10^6$ ($\delta\psi = -0.17, \delta\theta = 0.1, \delta H = 1.48$) ($H = 8.5$ was added).

Maximum heat transfer from fluid to solid occurs in the region close to the cold wall where the hot air, which moves horizontally towards the cold wall, touches the cold region of ceiling wall. The increase of the conductivity ratio causes a portion of heat which should be transferred to the cold wall transfers to the solid ceiling wall. Hence, the average Nusselt number of the cold vertical wall is reduced. The negative Nusselt number on the interface indicates a heat transfer from horizontal wall to the fluid on the left top corner of enclosure. It is obvious that for the enclosure with $K = 0$, the average Nusselt numbers of the hot and cold vertical walls are equal since no heat is transferred to the ceiling wall.

Fig. 6 depicts streamlines (on the left), isotherms (on the middle) and heatlines (on the right) for an enclosure with a thin horizontal wall, $D = 0.05$ and $K = 1$ for two Rayleigh numbers $Ra = 10^3$ (top row) and $Ra = 10^6$ (bottom row). A similar character of heat transfer of the enclosure with thick wall, $D = 0.5$, is observed. For $Ra = 10^3$, the convection effect in the enclosure is weak and the isotherms for the solid and fluid regions are nearly parallel to each others. It means that conduction is dominant due to low Rayleigh number. Almost one dimensional heat transfer exists in the ceiling wall of the enclosure. An increase of the Rayleigh number increases convection effect due to incoming energy. Hence, the average Nusselt number of the hot vertical wall increases.

To see the effects of conductivity ratio on the flow field, temperature distribution and heat transport of a thin ceiling wall enclosure, Fig. 7 is plotted for the same parameters of Fig. 6 except the thermal conductivity ratio which is $K = 100$. The solid body strongly conducts heat from the hot to cold vertical wall and acts like high conductive thermal bridge. Similar to the thick ceiling wall, the values of $|\psi|_{\max}$ and $\bar{N}u|_{X=0}$ (hot wall) increase however $\bar{N}u|_{X=1}$ (cold wall) decreases. The values of stream function and average Nusselt number of hot and cold vertical walls of the cavities with different K and D presented in Table 3 reveal that the effects of dimensionless wall thickness on the heat transfer through the cavity are less than the effects of K.

The variations of the average Nusselt number of the hot and cold vertical walls and also ceiling solid–fluid interface with thermal conductivity ratio for the enclosure with $D = 0.5$ and for the lowest and highest Rayleigh numbers are shown in Fig. 8. For $Ra = 10^6$, the average Nusselt number of hot vertical wall slightly rises with increase of thermal conductivity ratio in the region of low values of thermal conductivity (e.g. $K = 1$). The average Nusselt numbers of the solid–fluid interface also increases whereas $\bar{N}u|_{X=1}$ decreases. The increase of K causes the increase of heat transfer to the ceiling wall. For the cavities with high values of K, one dimensional heat transfer occurs in the horizontal wall and temperature variation is linear. Thus, the average Nusselt numbers of the solid–fluid interface, hot and cold vertical walls are not greatly changed. For $Ra = 10^3$, the increase of conductivity ratio does not greatly change temperature distribution in the enclosure since the convection heat transfer is weak and heat conduction in the wall of enclosure is almost one dimensional. As can be seen from Fig. 8, the average Nusselt numbers of hot and cold vertical walls and interface are almost constant for a wide range of conductivity ratio. These results also supported by Ben Yedder and Bilgen [6] for the differentially heated enclosures bounded by a solid vertical wall.

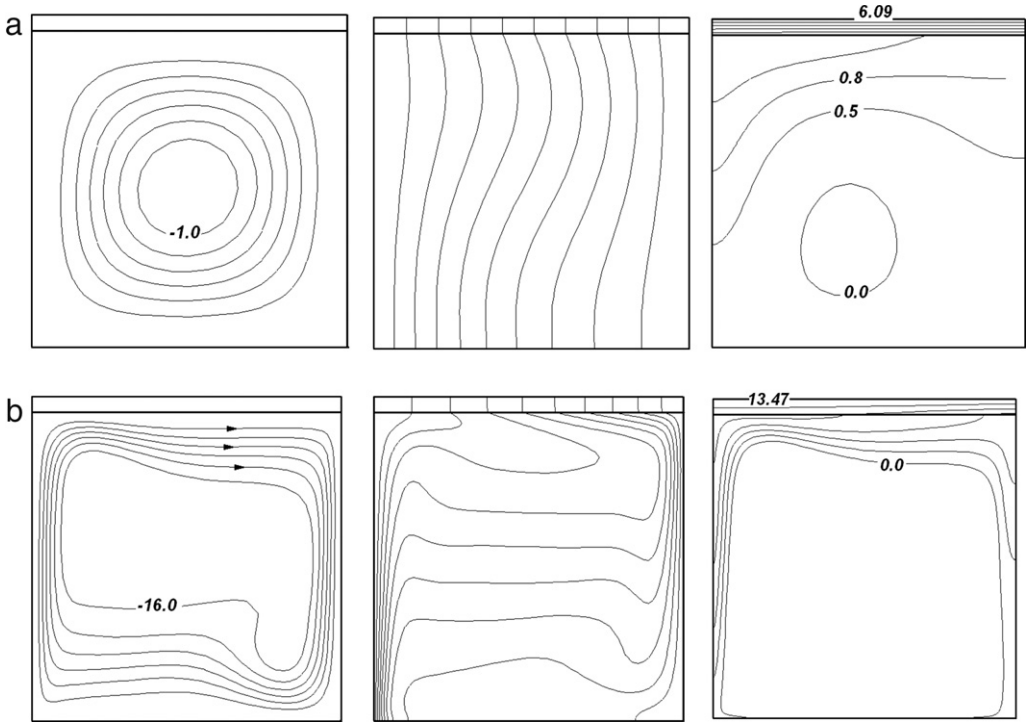

Fig. 7. Streamlines (on the left), isotherms (on the middle) and heatlines (on the right) in enclosure with $D = 0.05$ and $K = 100$ (a) $Ra = 10^3$, ($\delta\psi = -0.17$, $\delta\theta = 0.1$, $\delta H = 1.02$) ($H = 0.5$, 0.8 were added) (b) $Ra = 10^6$, ($\delta\psi = -0.17$, $\delta\theta = 0.1$, $\delta H = 2.45$).

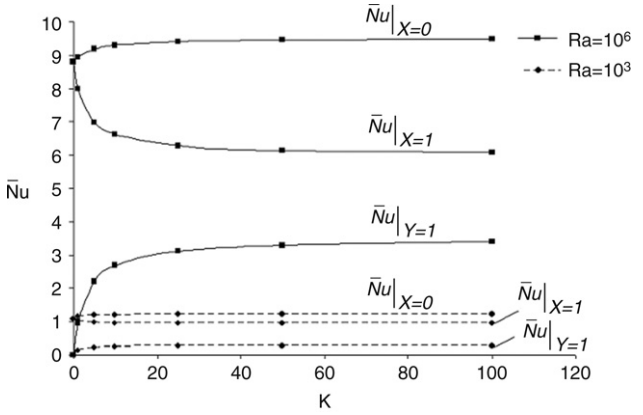

Fig. 8. Variation of average Nusselt number with thermal conductivity ratio for enclosure with $D = 0.5$.

The variations of average Nusselt number of hot and cold vertical walls and interface with the Rayleigh number are shown in Fig. 9 for $K = 0$, 1 and 100. The value of $\bar{N}u|_{X=0}$ (hot wall) increases with increasing of the Rayleigh number. The figure illustrates that the rate of increase of $\bar{N}u|_{X=0}$ in the enclosure with high values of K is greater. Fig. 9 also shows that heat transfer between solid and fluid on the interface enhances with increasing thermal conductivity ratio, on the contrary, the average Nusselt number of the cold vertical wall obviously decreases with increase of K. It should be mentioned that $\bar{N}u|_{X=0} = \bar{N}u|_{X=1}$ for $K = 0$, hence the corresponding curves overlap in Fig. 9.

7. Conclusion

From the results, our findings may be summarized as follows:

1. Heatline visualization technique is successfully employed to exhibit the direction and intensity of heat flux in the entire domain including solid and fluid regions. Heatlines are useful means for understanding mechanism of heat and fluid flows in a conjugate conduction-convection problem.

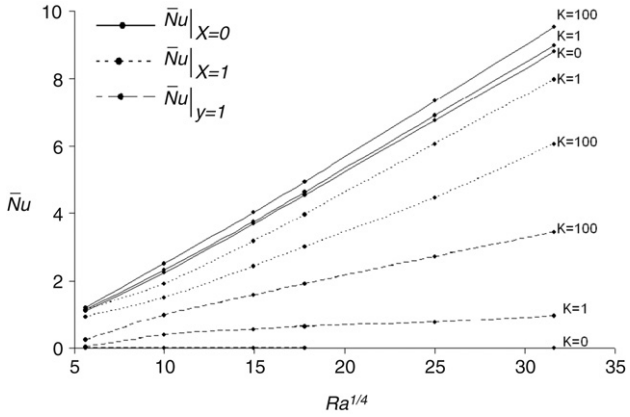

Fig. 9. Variation of average Nusselt number of hot and cold vertical walls and interface with Rayleigh number for enclosure with $D = 0.5$.

2. It is observed that, the dimensionless wall thickness does not greatly influence heat and fluid flow in a cavity and consequently heat transfer rate through the cavity is not considerably changed by ceiling wall thickness.
3. Heat transfer through the enclosure is influenced by thermal conductivity ratio. For an enclosure with low value of conductivity ratio ($K = 1$) and $Ra = 10^6$, the average Nusselt number of hot vertical wall slightly increases however the average Nusselt number of cold vertical wall decreases with increase of thermal conductivity ratio. The average Nusselt number of the interface also increases with increase of thermal conductivity ratio. All average Nusselt numbers do not significantly vary with high values of thermal conductivity ratio.
4. For an enclosure with $Ra = 10^3$, one dimensional heat transfer occurs in the horizontal wall and temperature distribution in the ceiling wall is almost linear even for high conductivity ratio (e.g. $K = 100$). Heat and fluid flows in the enclosure are not considerably changed with increase of thermal conductivity ratio.
5. The average Nusselt number of cold vertical wall increases by the Rayleigh number. The rate of increase is reduced by thermal conductivity ratio.

References

[1] S. Ostrach, Natural convection in enclosures, Adv. Heat Transfer 8 (1972) 161–227.
[2] S. Ostrach, Natural convection heat transfer in cavities and cells, in: Proc. 7th Int. Heat Transfer Conf., Toronto, Canada, 1978, pp. 143–149.
[3] G. De Vahl Davis, I.P. Jones, Natural convection in a square cavity: A comparison exercise, Internat. J. Numer. Methods Fluids 3 (1983) 227–245.
[4] D.M. Kim, R. Viskanta, Heat transfer by conduction, natural convection and radiation across rectangular cellular structure, Internat. J. Heat Fluid Flow 5 (1984) 205–212.
[5] R.B. Yedder, E. Bilgen, Turbulent natural convection and conduction in enclosures bounded by a massive wall, Internat. J. Heat Mass Transfer 38 (1995) 1879–1891.
[6] R.B. Yedder, E. Bilgen, Laminar natural convection in inclined enclosures bounded by a solid wall, Heat Mass Transfer 32 (1997) 455–462.
[7] D.A. Kaminski, C. Prakash, Conjugate natural convection in a square enclosure: Effect of conduction in one of the vertical walls, Internat. J. Heat Mass Transfer 29 (1986) 1979–1988.
[8] N.H. Saeid, Conjugate natural convection in a porous enclosure: Effect of conduction in one of the vertical walls, Int. J. Thermal Sci. 46 (2007) 531–539.
[9] N.H. Saeid, Conjugate natural convection in a vertical porous layer sandwiched by finite thickness walls, Int. Comm. Heat Mass Transfer 34 (2007) 210–216.
[10] F. Sanchez, F. Solorio, R. Avila, Conjugate natural convection in a square cavity heated from below, in: Proceedings of IMECE04, 2004 ASME Int. Mech. Eng. Congress and exposition, 1–10, Anaheim, CA, USA.
[11] H. Turkoglu, N. Yucel, Natural convection heat transfer in enclosures with conducting multiple partitions and side walls, Heat Mass Transfer 32 (1996) 1–8.
[12] B. Larbi, Statistical Modeling of Heat Transfer for Thermal Bridges of Buildings, in: Energy and Buildings, vol. 37, 2005, pp. 945–951.
[13] A.E. Ben Nakhi, Minimizing thermal bridging through window systems in buildings of hot regions, Appl. Thermal Eng. 22 (2002) 989–998.
[14] S.Y. Song, J.H. Jo, M.S. Yeo, Y.D. Kim, K.D. Song, Evaluation of Inside Surface Condensation in Double Glazing Window System with Insulation Spacer: A Case Study of Residential Complex, in: Building and Environment, vol. 42, 2007, pp. 940–950.
[15] P.F. Incropera, P.D. DeWitt, Fundamentals of Heat and Mass Transfer, fourth ed., John Wiley and Sons Inc., New York, 1996.
[16] S. Kimura, A. Bejan, The heatline visualization of convective heat transfer, ASME J. Heat Transfer 105 (1983) 916–919.
[17] O.V. Trevisan, A. Bejan, Combined heat and mass transfer in a vertical enclosure, ASME J. Heat Transfer 109 (1987) 104–112.
[18] A.M. Morega, A. Bejan, Heatline visualization of forced convection laminar boundary layers, Internat. J. Heat Mass Transfer 36 (1993) 3957–3966.
[19] V.A.F. Costa, Heatline and massline visualization of laminar natural convection boundary layers near a vertical wall, Internat. J. Heat Mass Transfer 43 (2000) 3765–3774.
[20] S.K. Dash, Heatline visualization in turbulent flow, Internat. J. Numer. Methods Heat Fluid Flow 5 (1996) 37–46.
[21] D.A. Nield, A. Bejan, Convection in Porous Media, second ed., Springer, New York, 1999.
[22] V.A.F. Costa, Bejan's heatlines and masslines for convection visualization and analysis, Appl. Mech. Rev. 59 (2006) 126–145.
[23] V.A.F. Costa, Unified streamline, heatline and massline methods for the visualization of two-dimensional heat and mass transfer in anisotropic media, Internat. J. Heat Mass Transfer 46 (2003) 1309–1320.
[24] M. Dalal, K. Das, Heatline method for the visualization of natural convection in a complicated cavity, Internat. J. Heat Mass Transfer 5 (2008) 263–272.
[25] Y. Jaluria, K. Torrence, Computational Heat Transfer, second ed., Taylor and Francis, 2003.
[26] M. Mobedi, Y. Yuncu, A three dimensional numerical study on natural convection heat transfer from short horizontal rectangular fin array, Heat Mass Transfer 39 (2003) 267–275.
[27] K.L. Wong, A.J. Baker, A 3D incompressible Navier–Stokes velocity vorticity weak form of finite element algorithm, Internat. J. Numer. Methods Fluids 38 (2002) 99–123.